RSC Advances

PAPER

View Article Online
View Journal | View Issue

Cite this: *RSC Adv.*, 2021, **11**, 32295

Leucomethylene blue probe detects a broad spectrum of reactive oxygen and nitrogen species†

Christopher Cremer, ‡[a] Jean Michél Merkes,‡[ab] Christina L. Bub, [a] Dirk Rommel,[c] Frederic W. Patureau [a] and Srinivas Banala *[abd]

Received 28th August 2021
Accepted 17th September 2021

DOI: 10.1039/d1ra06498c

rsc.li/rsc-advances

Reactive oxygen and nitrogen species (ROS, RNS) are ubiquitous in biology with a variety of physiological and pathological functions. Here we describe a broad spectrum ROS/RNS detecting fluorogenic probe with red fluorescence emission and up to 100-fold gain. Hence these modified probes are useful for *in vivo* non-invasive quantification of ROS/RNS.

Reactive oxygen species (ROS: $O_2^{\bullet -}$, H_2O_2, $HO^{\bullet}$, OCl^-, and $HO_2^{\bullet}$) and reactive nitrogen species (RNS: $ONOO^-$, $NO^{\bullet}$, NO_3^-) are classes of short-lived molecules produced in biological environments, *e.g.* in cellular metabolism, and in neutrophil actions.[1,2] They function as messengers, pathogen neutralizers, and play key roles in inducing inflammation,[3,4] and cancers.[5–7] Therefore, early non-invasive detection of ROS/RNS enable the onset of diseases. Several strategies, methods and probes are employed currently for the detection of ROS and RNS.[2,8–10] Electron paramagnetic resonance (EPR)[11] and fluorescence-based techniques are prevalent,[12] followed by photometric, chemiluminescent and electrochemical methods. In all these techniques, the applied probes change their properties post-reaction (or trapping) with ROS/RNS, and enable the detection.

Typically, many of above probes detect only one of the particular ROS/RNS species, and "overlook" those formed in earlier or subsequent metabolic steps, *e.g.* in EPR only radical species, in fluorescence and colorimetric techniques one type of ROS/RNS species. However, in biological systems the primarily produced ROS species (*e.g.* $O_2^{\bullet -}$) undergoes a variety of dissociation pathways forming secondary ROS species (see Fig. 1) and cause oxidative burden.[13] Thus, to estimate an overall oxidative stress, it is necessary to accurately assess the pathogenic levels production of all ROS/RNS species using a single probe.

Highly studied ROS detecting fluorogenic probes, 2′-7′-dichlorodihydrofluorescein (DCFH), its diacetate (DCFH-DA),[14] and dihydrorhodamine (DHR),[15] produce $O_2^{\bullet -}$ from O_2 after reaction with one-electron-oxidizing ROS/RNS species, *via* the radical ion ($DCFH^{\bullet -}$ or $DHR^{\bullet -}$). This catalytic formation of $O_2^{\bullet -}$, and its further conversion to other reactive species leads to an inaccurate detection of cellular ROS.[16] Further, the absorption and emissions wavelengths are incompatible for *in vivo* use.[17] It is optimal to have probes exhibiting optical properties in red-to-near infrared (NIR) range, where tissue auto fluorescence and phototoxicity are minimal. Towards such red-to-NIR emitting probes, previous studies employed reduced hydrocyanines, which undergo $HO^{\bullet}$ and $O_2^{\bullet -}$ mediated oxidation yielding red-to-NIR emitting cyanine dyes.[18] However the polymethine chain in cyanine itself is sensitive to oxidative cleavage with ROS species,[19,20] thus could lead to underestimation of ROS. Thus, new probes are of interest, which show high stability towards ROS, simultaneously exhibit fluorescence in red-to-NIR range.

Methylene blue (MB) dye has attracted our attention, as it exhibits absorption and emission in the biocompatible region,

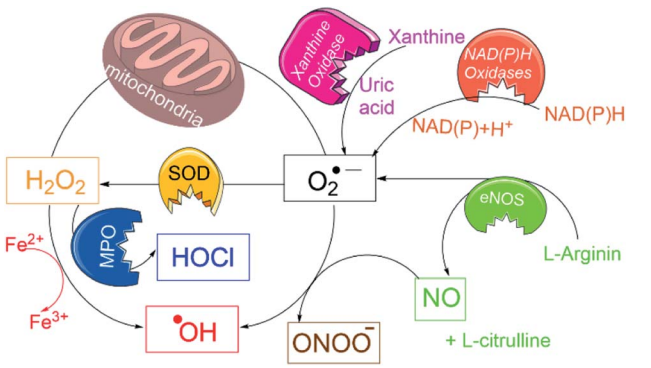

Fig. 1 Schematic overview for generation of a variety of ROS/RNS species in biological conditions and their interconversions.

[a]*Institute of Organic Chemistry, RWTH Aachen University, Landoltweg 1, Aachen, Germany*

[b]*Institute for Experimental Molecular Imaging, University Clinic, RWTH Aachen, Forckenbeckstrasse 55, Germany. E-mail: sbanala@ukaachen.de*

[c]*DWI-Leibnitz Institute for Interactive Materials and Institute for Technical and Macromolecular Chemistry, RWTH Aachen University, Forckenbeckstrasse 50, Aachen, Germany*

[d]*Fraunhofer Institute for Digital Medicine MEVIS, Max-von-Laue-Str. 2, 28359 Bremen, Germany*

† Electronic supplementary information (ESI) available. See DOI: 10.1039/d1ra06498c

‡ These authors contributed equally to the work.

at 665 nm and 686 nm, respectively.[21] Further, MB core is chemically modifiable,[22,23] and FDA-approved for therapeutic use,[24,25] and has been applied in a variety of applications, in disinfecting blood,[26] in treatment a variety of cancers,[27] as an antidote for methemoglobinemia[28] and in the photodynamic inactivation of bacteria,[25] funguses[29] and viruses.[30,31] These biological uses coupled with *in vivo* suitable optical properties make MB an attractive core the detection of ROS/RNS.

Recently, a reduced leucomethylene blue (LMB) was applied to selectively detect HOCl by formylating 10-N site (N^{10}-CHO) of LMB.[32] In another study, the N^{10}-site was modified with an enzyme[33] or light cleavable synthon,[34] which upon applying the respective trigger, yielded LMB and spontaneously oxidized to MB. We therefore are interested in modifying the LMB for detection of a broad spectrum of ROS/RNS species.

In our previous studies, we have identified that 2,6-di-*tert*-butyl phenol (BHP) moiety substituted dyes like porphyrins,[35] BODIPYs[36] reacted with a variety of ROS/RNS species, undergoing changes in their optical properties. The reactivity of BHP towards a variety of ROS/RNS is similar to that of the antioxidant 2,6-di-*tert*-butyl hydroxy toluene (BHT, a food additive),[37] as both share the same reactive site. Extending this strategy to LMB, we conceived to prepare a N^{10}-BHP appended LMB (BHP-LMB; **1**, **2**) for the ROS detection. As the BHP unit is hydrophobic, we approached a modification of LMB with polar groups like 1-butanesulfonate. Here we report the synthesis, and ROS detection characteristics as well as imaging applications of both constructs.

Towards the synthesis of the target BHP-LMB **1**, we employed a Buchwald–Hartwig C–N coupling, using reduced LMB and 4-iodo-2,6-*tert*-butylphenol (**6**). This method is appealing for its simplicity, as the C–N coupling chemistry has been extensively studied.[38] The C–N coupling reaction was performed in toluene with $Pd_2(dba)_3$ catalyst at 120 °C under nitrogen atmosphere (Scheme 1A). The BHP-LMB **1** could be isolated in 10% yield after column chromatography. Low yield was due to solubility of LMB in toluene, further sensitivity towards dissolved oxygen. Thus for purification of the coupling product **1**, N_2-gas was employed in chromatography, and the dye **1** could be obtained as pale-turquoise coloured solid after removal of the solvent. The HPLC and NMR showed >98% purity. The air-oxidation can be prevented by using reducing agents like citric acid, especially for spectroscopic measurements.

For the hydrophilic 1-butanesulfonylated BHP-LMB **2**, we have developed a second generation multi-step synthetic route starting from phenothiazine (PTZ). Towards **2**, we have first prepared a 2,8-diaminoacyl phenothiazine derivative (PTZ-NHAc, **3**) from 3,7-dinitro-10*H*-phenothiazine-5-oxide (see ESI†) as reported previously.[39] Then, for introducing the BHP unit at **3**, a convenient metal-free dehydrogenative amination method was applied based on a recently published route (Scheme 1B).[40] An advantage of this route is also the high stability of **3** and **4** towards oxygen. The following reduction of the acetyl groups in **4** was achieved using $BH_3{\cdot}SMe_2$ complex, obtaining mono ethyl BHP-PTZ derivative (**5**), which sets the stage for the final reaction towards the desired product **2**.

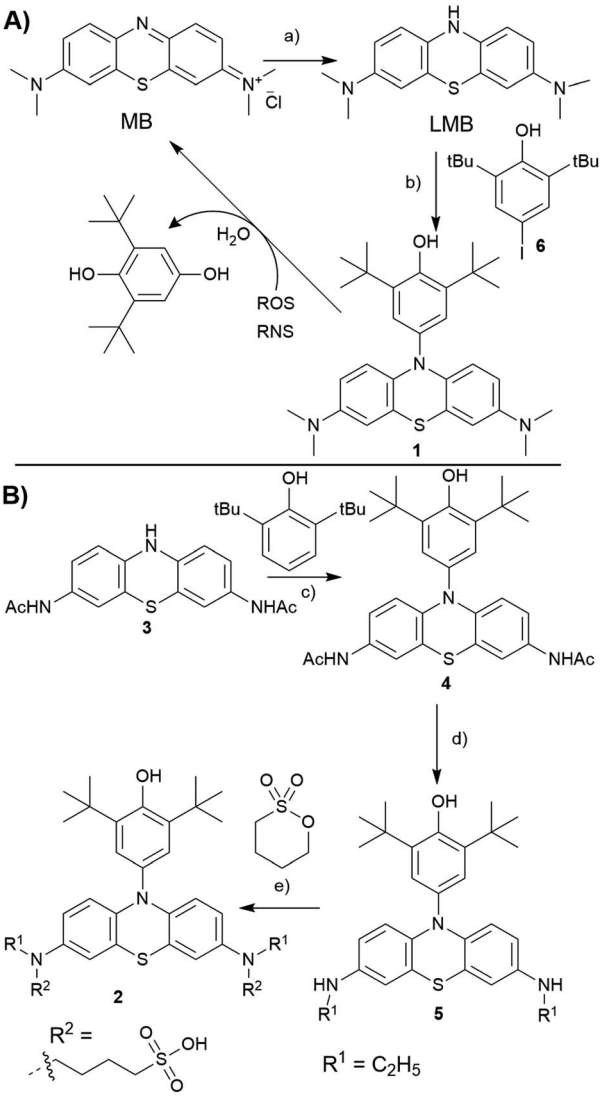

Scheme 1 (A) Synthesis of hydrophobic BHP-LMB (**1**), (B) bis-sultone added hydrophilic BHP-LMB (**2**). (a) K_2CO_3, $Na_2S_2O_4$ in DCM/H_2O at 40 °C under N_2, (60%) (b) $Pd_2(dba)_3$, DPPF, **6**, NaO^tBu in toluene at 110 °C under N_2, (10%, air sensitive) (c) $NaIO_4$ in DCM/AcOH, BHP, at 40 °C (34%); (d) $BH_3{\cdot}SMe_2$ in toluene at 110 °C (87%); (e) 1,4-butanesultone, DIPEA in MeCN at 80 °C under N_2 (15%).

Treating **5** with 1,4-butanesultone under basic conditions, by nucleophilic ring opening of the sultone, yielded 1-butanesulfonate attached BHP-LMB (**2**), along with mono sultone addition product. The hydrophilic product **2** was isolated by preparative RP-HPLC (reverse phase, with CH_3CN/H_2O gradient) as white solid after lyophilisation.

Having obtained two BHP-tethered probes **1** & **2**, we performed a screening with a variety of ROS/RNS by optical methods (Fig. 2; Fig. S1 and S2 in ESI† for titrations). The absorption (UV-vis) spectra of compounds were obtained, **1** in DMSO and of **2** in water; both BHP-LMBs showed a similar reactivity towards ROS, yielding MB as the final compound, though some peculiarities were observed. The $O_2^{\bullet-}$ was found to be highly aggressive especially in DMSO with **1**, compared to

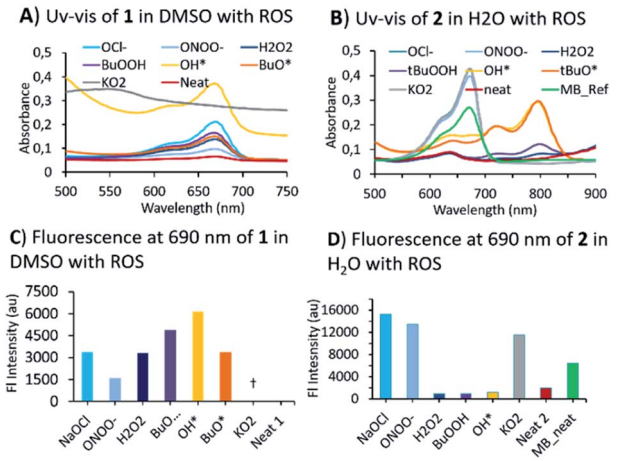

Fig. 2 Optical properties of MB-BHT (25 nmol mL^{-1}) after treating sufficient amount of ROS (>5 equiv.). Fluorescence emission (concentration 12 nmol mL^{-1}) at the maximum of 689 nm for excitation at 645 nm (†: due to fast decomposition of the formed MB).

2 in water. In DMSO, the $O_2^{\bullet-}$ reaction yielded MB instantly, that underwent decomposition in the presence of excess $O_2^{\bullet-}$. We investigated this reaction by NMR spectroscopy to identify any intermediates towards MB, using **1** titration with $O_2^{\bullet-}$ and MB with $O_2^{\bullet-}$, but found no stable species (Fig. S5†). However, during the treatment with OH$^{\bullet}$ and ^{t}BuO$^{\bullet}$ species, it was found that **2** in water gave a persistent far-red absorbing species which was not observed in DMSO with **1** (Fig. S3† *versus* Fig. S1†). Similar spectral features were observed with H_2O_2 and tBuOOH towards **2** in H_2O albeit with a lower intensity, but not with **1** in DMSO. This is presumably, a relatively stable BHP-radical appended LMB formed in water but not in DMSO (Fig. S3†). For anionic ROS species, $O_2^{\bullet-}$, $ONOO^-$ and OCl^-, the absorption and fluorescence emission are consistent in both solvents with a small discrepancy in the gain ratio. This can be attributed to a different rate of reaction for formation of MB. In treating **1** with RNS species, NO_2^- and NO_3^- in DMSO, resulted MB (Fig. S2†). These optical characteristics confirm that **1** and **2** exhibit a good sensitivity towards most of the ROS/RNS species and are thus suitable for estimating overall oxidative stress.

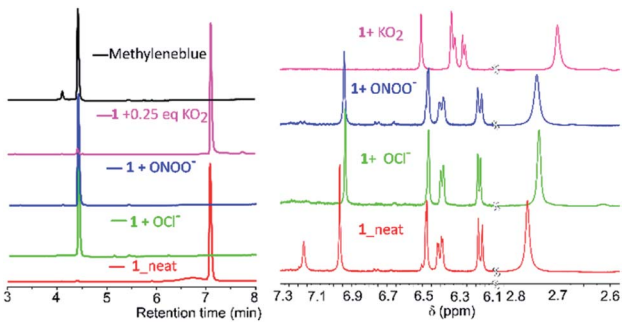

Fig. 3 (A) HPLC chromatograms (detection at 254 nm; along with MB and neat **1**) and (B) NMR-spectra (in DMSO-d_6) for addition of $O_2^{\bullet-}$, $ONOO^-$, OCl^- species to **1** in D_2O/H_2O to the DMSO-d_6.

Mechanistic investigations into the formation of intermediates were conducted by HPLC and NMR (Fig. 3). Here, **1** was treated with $ONOO^-$, OCl^-, $O_2^{\bullet-}$ as they were found to be consistent in both solvents. Adding $ONOO^-$ and OCl^- in excess to **1** gave a clean MB product without any trace of other species (Fig. 3A). Treatment of **1** with a minimal amount of $O_2^{\bullet-}$ showed existence of both **1** and MB traces in HPLC. For NMR titrations, to a DMSO-d_6 solution of **1**, ROS species in D_2O were added. For addition of $O_2^{\bullet-}$, the chemical shifts corresponding to MB are downfield shifted slightly compared to $ONOO^-$, OCl^-. Furthermore, the NMR signals of the cleaved BHP unit were upfield shifted for $O_2^{\bullet-}$ than $ONOO^-$, OCl^- addition (Fig. 3B). This could indicate that the formed by-product, ^{t}Bu-hydroquinol, might have been further oxidized to a ^{t}Bu-quinone with $O_2^{\bullet-}$, but with $ONOO^-$, OCl^- persistent ^{t}Bu-hydroquinol. Nevertheless, as no other intermediate species were detected in HPLC, and all ROS produced MB as the final compound, **1** could be suitable for detecting all the ROS species.

Having characterized the ROS reactions of **1** and **2** in the formation of MB, we focused on imaging the cellular produced ROS by confocal laser scanning microscopy. For this, we chose the established ROS-producing macrophage cell line J774.A1, which express ROS when treated with lipopolysaccharide (LPS) and interferon-γ (IFN-γ).

The cells attached to coverslips were treated with LPS and IFN-γ, incubated for 24 hours to induce ROS. To these activated cells in 1 mL medium, 10 nmol of BHP-LMB **1** or **2** was added as DMSO or phosphate buffered saline (PBS) solution, respectively, and incubated for 6 h. The cells were fixated with 4% formalin, washed PBS and mounted on glass slides with Mowiol for microscopy. The membrane labelling WGA-488 probe was used additionally for reference. For control cells, no ROS induction was carried out with LPS/IFN-γ (Fig. 4, top). In addition, the hydrophobic **1** incorporated controlled cells, after formalin fixation, were treated with $ONOO^-$ for 30 min, and washed with PBS (Fig. 4, bottom) to characterize the activation of intracellularly accumulated **1**. This confirmed intra-cellularization of **1** and trapping the cellular produced ROS (Fig. 4, middle panel) or the added ROS by BHP-LMB **1** yielding red-emitting MB. A similar procedure was performed with **2**, and microscopy imaging confirmed that there was no fluorescence (Fig. S4†) indicating the dye **2** was not intracellularized.

In summary, here we described broad-spectrum ROS/RNS detecting probes based on 2,6-di-*tert*-butyl phenol (BHP) appended leuco-methylene blue (BHP-LMBs, **1**, **2**). Hydrophobic **1** and hydrophilic **2** are sensitive towards a variety of ROS and RNS, producing the red fluorescent MB. *In vitro* titration with a variety of ROS showed formation of MB from **1** in DMSO, and also a persistent far red-absorbing radical species from **2** in H_2O. The NMR and HPLC analysis of **1** in DMSO with $O_2^{\bullet-}$, $ONOO^-$ and OCl^- showed no stable intermediates *en route* to MB. Then **1** was employed in detecting cellular produced ROS by fluorescence microscopy, which confirmed its intracellularization and suitability for detecting cellular generated ROS. The hydrophilic **2** found to be not intracellularized, and hence it may be used for extracellularly diffused ROS detection. These results suggest the suitability of

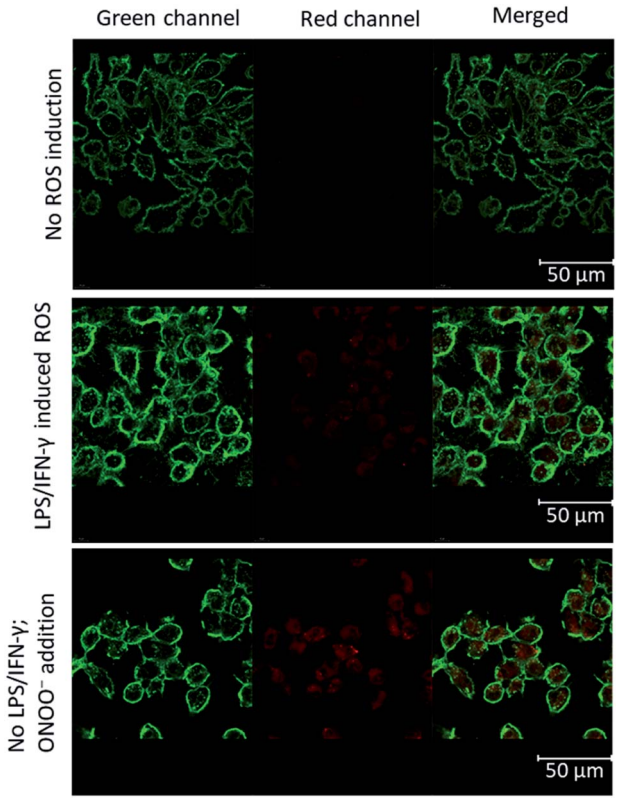

Fig. 4 Confocal microscopy images using **1** and J774.A1 cells for the detection of ROS; top: without ROS induction; middle: ROS expression induced by LPS/IFN-γ; bottom with $ONOO^-$ addition to the fixed cells (conc: 10 nmol mL^{-1} of **1**, 6 h incubation; green: membrane labelling probe WGA-488 (exc. 488 nm), red: **1** after ROS reaction (exc. 660 nm).

1, **2** in broad spectrum *in vivo* detection of ROS, which will be explored in future studies.

Author contributions

The manuscript was written through contributions of all authors. C. C., C. L. B. performed synthesis and analysis. J. M. M, S. B. performed cellular experiments, spectroscopic studies, and D. R. the microscopy. S. B. proposed and coordinated the research with F. W. P, analysed the results and wrote the manuscript. All authors have given approval to the final version of the manuscript.

Conflicts of interest

There are no conflicts to declare.

Acknowledgements

S. B. acknowledges financial support from Excellent Initiative of the German federal and state governments through the I3TM Seed Fund and I3TM Step2Projects, F. W. P. acknowledges the financial support from European Research Council for project 716136: "2O2ACTIVATION".

Notes and references

1 *Reactive Oxygen Species in Biology and Human Health*, ed.S. I. Ahmad, CRC Press, New York, 2016.
2 J.-T. Hou, K.-K. Yu, K. Sunwoo, W. Y. Kim, S. Koo, J. Wang, W. X. Ren, S. Wang, X.-Q. Yu and J. S. Kim, *Chem*, 2020, **6**, 832–866.
3 S. Dikalov, K. K. Griendling and D. G. Harrison, *Hypertension*, 2007, **49**, 717–727.
4 S. Di Meo, T. T. Reed, P. Venditti and V. M. Victor, *Oxid. Med. Cell. Longevity*, 2016, **2016**, 1245049.
5 P. T. Schumacker, *Cancer Cell*, 2006, **10**, 175–176.
6 S. Kumari, A. K. Badana, G. Murali Mohan, G. Shailender and R. R. Malla, *Biomarker Insights*, 2018, **13**, 1177271918755391.
7 C. R. Reczek and N. S. Chandel, *Annu. Rev. Cancer Biol.*, 2017, **1**, 79–98.
8 X. Bai, K. K.-H. Ng, J. J. Hu, S. Ye and D. Yang, *Annu. Rev. Biochem.*, 2019, **88**, 605–633.
9 Y. Zhang, M. Dai and Z. Yuan, *Anal. Methods*, 2018, **10**, 4625–4638.
10 E. M. Espinoza, J. J. Røise, I. C. Li, R. Das and N. Murthy, *J. Nucl. Med.*, 2021, **62**, 457–461.
11 P. L. Zamora and V. F. A. Røise, in *Measuring Oxidants and Oxidative Stress in Biological Systems*, ed. L. Berliner and N. L. Parinandi, Springer, Cham, 2020, vol. 34, pp. 13–38.
12 L. Wu, A. C. Sedgwick, X. Sun, S. D. Bull, X.-P. He and T. D. James, *Acc. Chem. Res.*, 2019, **52**, 2582–2597.
13 P. Wardman, *Free Radical Biol. Med.*, 2007, **43**, 995–1022.
14 S. L. Hempel, G. R. Buettner, Y. Q. O'Malley, D. A. Wessels and D. M. Flaherty, *Free Radical Biol. Med.*, 1999, **27**, 146–159.
15 P. Wardman, in *Methods in Enzymology*, ed. E. Cadenas and L. Packer, Academic Press, 2008, vol. 441, pp. 261–282.
16 M. G. Bonini, C. Rota, A. Tomasi and R. P. Mason, *Free Radical Biol. Med.*, 2006, **40**, 968–975.
17 B. Kalyanaraman, V. Darley-Usmar, K. J. A. Davies, P. A. Dennery, H. J. Forman, M. B. Grisham, G. E. Mann, K. Moore, L. J. Roberts and H. Ischiropoulos, *Free Radical Biol. Med.*, 2012, **52**, 1–6.
18 K. Kundu, S. F. Knight, N. Willett, S. Lee, W. R. Taylor and N. Murthy, *Angew. Chem., Int. Ed.*, 2009, **48**, 299–303.
19 Q. Zheng, S. Jockusch, Z. Zhou and S. C. Blanchard, *Photochem. Photobiol.*, 2014, **90**, 448–454.
20 G. W. Byers, S. Gross and P. M. Henrichs, *Photochem. Photobiol.*, 1976, **23**, 37–43.
21 J. P. Tardivo, A. Del Giglio, C. S. de Oliveira, D. S. Gabrielli, H. C. Junqueira, D. B. Tada, D. Severino, R. de Fátima Turchiello and M. S. Baptista, *Photodiagn. Photodyn. Ther.*, 2005, **2**, 175–191.
22 S. P. Massie, *Chem. Rev.*, 1954, **54**, 797–833.
23 E. P. Guttmann, *Berl. Klin. Wochenschr.*, 1891, **28**, 953–956.
24 M. Wainwright and K. B. Crossley, *Chemother. J.*, 2002, **14**, 431–443.
25 R. Boltes Cecatto, L. Siqueira de Magalhães, M. Fernanda Setúbal Destro Rodrigues, C. Pavani, A. Lino-dos-Santos-

Franco, M. Teixeira Gomes and D. Fátima Teixeira Silva, *Photodiagn. Photodyn. Ther.*, 2020, **31**, 101828.
26 H. Mohr, B. Lambrecht and A. Selz, *Immunol. Invest.*, 1995, **24**, 73–85.
27 X. Jin, H. Xu, J. Deng, H. Dan, P. Ji, Q. Chen and X. Zeng, *Photodiagn. Photodyn. Ther.*, 2019, **28**, 146–152.
28 Y. Yusim, D. Livingstone and A. Sidi, *J. Clin. Anesth.*, 2007, **19**, 315–321.
29 J. J. Shen, G. B. E. Jemec, M. C. Arendrup and D. M. L. Saunte, *Photodiagn. Photodyn. Ther.*, 2020, **31**, 101774.
30 T.-W. Wong, H.-J. Huang, Y.-F. Wang, Y.-P. Lee, C.-C. Huang and C.-K. Yu, *J. Antimicrob. Chemother.*, 2010, **65**, 2176–2182.
31 Q. Huang, W.-L. Fu, B. Chen, J.-F. Huang, X. Zhang and Q. Xue, *J. Photochem. Photobiol., B*, 2004, **77**, 39–43.
32 P. Wei, W. Yuan, F. Xue, W. Zhou, R. Li, D. Zhang and T. Yi, *Chem. Sci.*, 2018, **9**, 495–501.
33 J. Bae, L. E. McNamara, M. A. Nael, F. Mahdi, R. J. Doerksen, G. L. Bidwell, N. I. Hammer and S. Jo, *Chem. Commun.*, 2015, **51**, 12787–12790.
34 H. M. Dao, C.-H. Whang, V. K. Shankar, Y.-H. Wang, I. A. Khan, L. A. Walker, I. Husain, S. I. Khan, S. N. Murthy and S. Jo, *Chem. Commun.*, 2020, **56**, 1673–1676.
35 J. M. Merkes, M. Rueping, F. Kiessling and S. Banala, *ACS Sens.*, 2019, **4**, 2001–2008.
36 J. M. Merkes, A. Hasenbach, F. Kiessling, S. Hermann and S. Banala, Unpublished work, 2021.
37 W. A. Yehye, N. A. Rahman, A. Ariffin, S. B. Abd Hamid, A. A. Alhadi, F. A. Kadir and M. Yaeghoobi, *Eur. J. Med. Chem.*, 2015, **101**, 295–312.
38 P. Ruiz-Castillo and S. L. Buchwald, *Chem. Rev.*, 2016, **116**, 12564–12649.
39 R. Jin, C. L. Bub and F. W. Patureau, *Org. Lett.*, 2018, **20**, 2884–2887.
40 R. Jin and F. W. Patureau, *Org. Lett.*, 2016, **18**, 4491–4493.